ELSEVIER

Catalysis Today 76 (2002) 161–175

CATALYSIS TODAY

www.elsevier.com/locate/cattod

Photocatalytic reactors
Reaction kinetics in a flat plate solar simulator

Rodolfo J. Brandi, Gerardo Rintoul, Orlando M. Alfano, Alberto E. Cassano*

INTEC (CONICET and Universidad Nacional del Litoral), Güemes 3450, 3000 Santa Fe, Argentina

Abstract

The kinetics of the photocatalytic decomposition of low concentrations of trichloroethylene (TCE) in water was modeled and the reaction parameters have been evaluated for different catalyst loadings. The employed reactor is a flat plate configuration irradiated by tubular lamps that have emission in the 300–400 nm wavelength range.

The mass conservation model is two-dimensional while the developed radiation model is two-dimensional in space and two directional in radiation propagation. The performance of the photoreactor with this reaction can be properly represented employing only two lumped kinetic constants that can be derived from a 12 steps, complete reaction sequence. The deduced kinetic model has explicit functional dependencies for the local volumetric rate of photon absorption (LVRPA) and the effect of the catalyst concentration: $r_{\mathrm{TCE,het}}(x,t)a_{\mathrm{v}} = -S_{\mathrm{g}}\sqrt{C_{\mathrm{m,cat}}}\alpha\left[\sqrt{\int_{\lambda} e^{\mathrm{a}}_{\lambda}(x,t,C_{\mathrm{m,cat}})\,\mathrm{d}\lambda}\right][\alpha_3 C_{\mathrm{TCE}}/(1+\alpha_3 C_{\mathrm{TCE}})]$. Values of the kinetic constants are: $\alpha = 1.94\times10^{-9}$ mol g$^{1/2}$ cm^{-2} s$^{-1/2}$ einstein$^{-1/2}$ and $\alpha_3 = 5.52\times10^{6}$ cm^3 mol^{-1}. As derived from the reaction sequence and validated with experiments, it was observed that the reaction rate is proportional to the square root of the LVRPA. The dependence on the catalyst loading, well described by the model, is more complex due to its characteristic effect on the light distribution inside the reaction space.

Keywords: UV radiation; Photocatalysis; Reaction kinetics; Flat plate reactor; Trichloroethylene

1. Introduction

Photocatalytic reactions are a family of the new advanced oxidation technologies employing titanium dioxide and UV radiation with potential applications in water and air purification. The applied radiation may be artificial or solar light. In respect of the last, it has been precisely shown that flat plate collectors are more efficient than parabolic trough reactors [1]; i.e., it is convenient to use reactors that have the ability to collect also the diffuse part of solar irradiation. Thus, understanding the performance of this type of reactors becomes an important issue in photocatalytic reactor design. In these processes, the rate of electron–hole generation—the catalyst activation step—is always a function of the local volumetric rate of photon absorption (LVRPA). In heterogeneous systems with suspended solids (the catalyst) its evaluation is more complex due to the simultaneous existence of radiation absorption and scattering.

In this work, a model for describing the kinetic performance of a flat plate photocatalytic reactor employed for the degradation of trichloroethylene (TCE) is presented. The reacting system is made of: (i) a thin rectangular parallelepiped limited by two parallel planes made of borosilicate glass that operates inside

* Corresponding author. Tel.: +54-342-4559175; fax: +54-342-4559185.
E-mail address: acassano@alpha.arcride.edu.ar (A.E. Cassano).

0920-5861/02/$ – see front matter © 2002 Elsevier Science B.V. All rights reserved.
PII: S0920-5861(02)00216-X

Nomenclature

a_v	solid–liquid interfacial area per unit reactor volume ($m^2\,m^{-3}$)
A	area (m^2)
C_i	molar concentration of component i ($mol\,m^{-3}$)
C_m	mass concentration ($g\,m^{-3}$)
e^a	volumetric rate of photon absorption ($einstein\,s^{-1}\,m^{-3}$)
H	depth (m)
I	specific (radiation) intensity ($einstein\,s^{-1}\,m^{-2}\,sr^{-1}$)
L	length (m)
LVRPA	local volumetric rate of photon absorption ($einstein\,s^{-1}\,m^{-3}$)
p	phase function (dimensionless)
Q	volumetric flow rate ($m^3\,s^{-1}$)
r_{het}	heterogeneous reaction rate ($mol\,s^{-1}\,m^{-2}$)
S_g	catalyst surface area ($m^2\,g^{-1}$)
t	time (s)
T	transmittance (dimensionless)
v	velocity ($m\,s^{-1}$)
V	volume (m^3)
W	width (m)
x	Cartesian coordinate (m)
$\underline{x}$	vector representing position in a 3D space (m)
y	Cartesian coordinate (m)
z	Cartesian coordinate (m)

Greek letters

α	kinetic parameter defined by Eq. (13) ($mol\,cm^{-2}\,g^{1/2}\,s^{-1/2}\,einstein^{-1/2}$)
α_1	kinetic parameter ($mol\,cm^{-2}\,s^{-1}$)
α_2	kinetic parameter ($g\,s\,einstein^{-1}$)
α_3	kinetic parameter ($cm^3\,mol^{-1}$)
β	extinction coefficient (cm^{-1})
β^*	specific extinction coefficient ($cm^2\,g^{-1}$)
ε_L	liquid hold-up (dimensionless)
η	direction cosine ($= \sin\theta \sin\phi$)
θ	spherical coordinate (rad)
ϑ	angle between radiation rays defined for the diffuse phase function (rad)
κ	absorption coefficient (cm^{-1})
κ^*	specific (per unit mass) absorption coefficient ($cm^2\,g^{-1}$)
λ	wavelength ($nm = 10^{-9}\,m$)
μ	direction cosine ($= \sin\theta \cos\phi$)
σ	scattering coefficient (cm^{-1})
σ^*	specific scattering coefficient ($cm^2\,g^{-1}$)
τ	mean residence time (s)
ϕ	spherical coordinate (rad)
Ω	solid angle (sr)
$\underline{\Omega}$	unit vector in the direction of radiation propagation

Subscripts

A	area
cat	catalyst
in	solid angle of incoming radiation
L	liquid phase
max	maximum value
R	reactor
t_l	load time
Tk	tank
x	relative to x-axis
λ	wavelength

Superscripts

in	inlet condition
ou	outlet condition
0	initial value
$*$	specific (per unit mass) properties

Special symbols

$\underline{\ }$	vector value
$\langle\cdot\rangle$	average value

a closed recycling system, (ii) two "actinic" type, tubular UV lamps, and (iii) two parabolic reflectors housing the tubular lamps at their focal axis. Both the chemical system and the reactor have been the subject of previous studies.

The photocatalytic degradation kinetics of TCE was investigated in detail by Alfano et al. [2] and Cabrera et al. [3] in the presence of an excess of oxygen over the stoichiometric demand. Polychromatic light from 300 to 400 nm in wavelength and a batch of commercial Aldrich titanium dioxide were used. Employing

a wavelength averaged quantum yield for the rate of electron–hole generation the kinetics was modeled with a reaction sequence of 12 steps previously proposed by Turchi and Ollis [4] that considers that the most important degradation mechanism is based on the $OH^{\bullet}$ radical attack on the hydrocarbon. The kinetic model has only three lumped parameters that were adjusted with experimental data and includes an explicit description of the reaction rate dependence with the LVRPA. It was clearly stated [5] that the model has some limitations; among them we can list: (1) all adsorption processes have been assumed to be in equilibrium, (2) the model does not include the effect of oxygen on the rate, (3) since the effect of wavelength on the quantum yield for electron–hole generation was not taken into account by the model, changes in the spectral distribution of the employed light could affect the validity of the calculated parameters, (4) the model used a diffuse phase function for describing scattering while it has been known just recently that scattering by titanium dioxide is better represented by an isotropic function [6], (5) also, the same diffuse phase function was used in that work to calculate, from independent experiments the absorption and scattering coefficients, (6) the non-linear parameter estimator was applied to a chemical model in which effects produced on the rate by the reaction products have not been considered, and (7) the obtained kinetic parameters are certainly valid only for the batch of titanium dioxide employed in that work.

The radiation field in the flat plate, photocatalytic reactor employing a suspension of both Aldrich and Degussa P 25 titanium dioxide was also studied in detail by Brandi et al. [6,7]. It was found that: (1) radiation profiles inside the reactor with one or the other catalyst are significantly different, (2) with both catalysts, even for concentrations as low as 0.5 g/l, after 1 cm of reactor thickness the reaction space becomes almost opaque, (3) from the radiation capture point of view, the Aldrich catalyst is more efficient due to the higher loss of radiation produced by scattering in the Degussa P 25 case, and (4) fouling of the reactor walls is very important when Degussa P 25 is employed. Along this work, it was also shown that scattering by titanium dioxide is better modeled when an isotropic phase function for scattering is used. No kinetic studies were carried out in this reactor.

The developed model of this work consider separated mass balances for each of the two reservoirs, i.e., for the reactor and the storage tank of the recycle. The mass balance for the reactor is two-dimensional and the mathematical representation of the radiation field for the heterogeneous reaction space is two-dimensional–two directional. This model ameliorates on previous work in the following aspects: (i) the phase function for scattering—that better represents the behavior of titanium dioxide has been used for solving the radiation problem (the isotropic function), (ii) the optical properties of the suspension have been calculated with the isotropic phase function, (iii) the simplification of diffuse irradiating boundary condition has been removed allowing to eliminate the azimuthal symmetry approximation, and (iv) the effect of catalyst particle agglomeration that changes the optical properties of the reacting medium and hence the light distribution inside the reactor has been taken into account. Other important differences are: (i) the employed lamp, with UV emission in the 300–400 nm wavelength range, better resembles solar irradiation and (ii) because the operation is conducted in a larger reactor size, the assumption of perfectly mixed system in the photocatalytic reaction space was withdrawn and substituted by a two-dimensional representation; thus, the last change leads to a different reactor model to interpret the experimental results. The kinetic model of this work was obtained with an extension of the previous one [2] valid for the irradiation rates employed in this study. With a non-linear parameter estimator the two lumped constants of the new model were obtained in an expression that shows the explicit dependence of the rate with respect to the LVRPA and the catalyst concentration.

2. Reactor model

2.1. Mass balances

Schematically, the system under study is formed by a photoreactor of volume V_R and a tank of volume V_{Tk} functioning in a closed circuit (Fig. 1). The tank operates under unsteady state conditions. The mass balance in the tank for a generic species i is represented by the following differential equation and initial

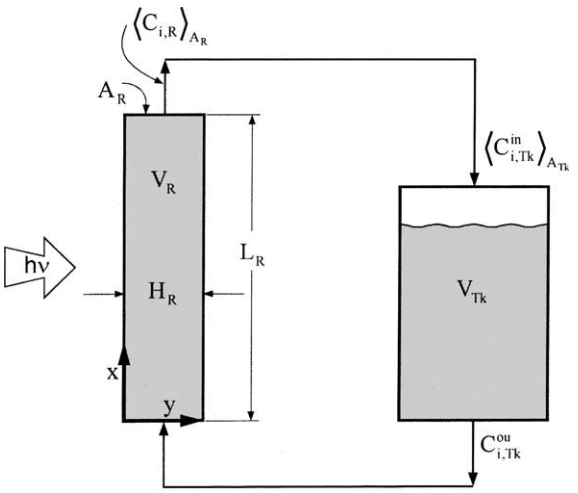

Fig. 1. Schematic representation of the employed system.

condition:

$$\varepsilon_L \frac{dC^{ou}_{i,Tk}}{dt} = \frac{1}{\tau_{Tk}}[\langle C^{in}_{i,Tk}(x,t)\rangle_{A_{Tk}} - C^{ou}_{i,Tk}(t)] \quad (1)$$

$$C^{ou}_{i,Tk}(t=0) = C^0_i \quad (2)$$

In Eq. (1) the mean residence time in the tank is given by $\tau_{Tk} = V_{Tk}/Q$. It will be seen in the description of the operating conditions (Section 3.1) that the tank works under well-stirred conditions. Hence the concentration in the tank (equal to its outlet concentration) is only a function of time. The inlet concentration in the tank comes from the reactor. The exit concentration from the reactor is also an exclusive function of time after it has been averaged over the reactor outlet cross-sectional area. This concentration is not known. One can safely assume that

$$\langle C^{in}_{i,Tk}(x,t)\rangle_{A_{Tk}} = \langle C_{i,R}(L_R,y,t)\rangle_{A_R} \quad (3)$$

This means that the average exit concentration from the reactor equals the average inlet concentration to the tank.

To know the right hand concentration in Eq. (3) we need a mass balance in the photoreactor. The reactor functions under the following conditions: (i) pseudo-steady state, with an inlet concentration that is a function of time (we are assuming that during one reactor mean residence time, which is very short, the outlet concentration from the tank remains practically unchanged), (ii) laminar flow, (iii) concentration variations along the *z*-direction are not important, and (iv) there is no mixing along the directions *x*, *y* and *z*. This last condition results from: (1) the symmetry existing in the *z*-direction, (2) the uniform radiation field existing along the *x*-direction, (3) the laminar flow existing in the reactor, and (4) the low diffusion fluxes expected in the liquid phase. Thus, neglecting diffusive fluxes, the mass balance for generic a species *i* is represented by the following differential equation and inlet condition (at $x = 0$):

$$v_{max}\left[1 - \left(\frac{2y}{H_R} - 1\right)^2\right]\varepsilon_L \frac{\partial C_{i,R}(x,y,t)}{\partial x} = \nu_i r_{het}(x,y,t) a_v \quad (4)$$

$$C_{i,R}(x=0,y,t) = C^{ou}_{i,Tk}(t) \quad (5)$$

In Eq. (4) the maximum velocity in laminar flow is given by

$$v_{max} = \frac{3}{2}\frac{Q}{H_R W_R} \quad (6)$$

The employed velocity profile has been assumed to be valid for this work considering that the characteristics of the titanium dioxide and the operating catalyst concentration (≤0.1%) will not affect sensibly the Newtonian behavior of the solvent.

Solving Eqs. (4) and (5) we get concentrations of the species *i* as a function of *x*, *y* and *t*. The average exit concentration from the reactor is then obtained from

$$\langle C_{i,R}(L_R,y,t)\rangle_{A_R} = \frac{\int_{y=0}^{y=H_R} C_{i,R}(L_R,y,t) v_x(y)\,dy}{\int_{y=0}^{y=H_R} v_x(y)\,dy} \quad (7)$$

Concentrations calculated with Eq. (7) are only a function of time. It becomes now clear that to calculate the concentration in the tank where sampling is made $C_{i,Tk}(t) = C^{ou}_{i,Tk}(t)$, we must solve the set of Eqs. (1)–(7).

2.2. Reaction rate

As said in Section 1 the degradation rate of TCE will be analyzed. A kinetic model for the photocatalytic

degradation of TCE has been published in [2,3]. The general expression for the heterogeneous photocatalytic degradation of TCE (i = TCE) is

$$r_{i,\mathrm{het}}(\underline{x},t) = -\alpha_1 \left(\frac{\alpha_3 C_i(\underline{x},t)}{1+\alpha_3 C_i(\underline{x},t)}\right)\left[-\left(\frac{\alpha_3 C_i(\underline{x},t)}{1+\alpha_3 C_i(\underline{x},t)}\right) + \sqrt{\left(\frac{\alpha_3 C_i(\underline{x},t)}{1+\alpha_3 C_i(\underline{x},t)}\right)^2 + \frac{\alpha_2}{C_{\mathrm{m,cat}}}\int_\lambda e^{\mathrm{a}}_\lambda(\underline{x},t,C_{\mathrm{m,cat}})\,\mathrm{d}\lambda}\right] \tag{8}$$

The rate described by Eq. (8) is a function of the spatial coordinates ($\underline{x}$) and time (t). This functionality results from the following circumstances: (i) along the degradation experiment TCE concentration in the recycling system changes with time, (ii) the reactor has not been assumed to operate under well mixing conditions and consequently concentrations are not uniform in space, (iii) the rate of electron–hole generation, that is directly proportional to the LVRPA, is a strong function of position and time due to two different factors: (iiia) radiation absorption by the catalyst is very strong and generates a radiation field that varies very much in the y-direction and (iiib) the radiation field is also a function of time because the optical properties of the catalytic suspension vary with time [8]. This last aspect changes the absorption of photons by the reacting medium, an effect that has not been considered in the modeling of these photoreactors so far.

It is interesting to note that a kinetic statement such as Eq. (8) comprises the two limiting cases that are usually reported in photocatalytic reaction rates at low and medium to high irradiation rates. It has been shown that at medium to high values of the LVRPA, Eq. (8) renders a rate that is proportional to the square root of the LVRPA and at low values of the LVRPA, Eq. (8) will reproduce a reaction rate that is proportional to the LVRPA [2]. It is also clear that a complete representation such as the one described by Eq. (8) will also explain the existing intermediate behavior between low to medium/high irradiation rates; a situation that should be expected to occur at practical catalyst concentrations between a region close to the surface of radiation entrance (high LVRPA) and a region where most of the incoming radiation has already been absorbed or scattered (low LVRPA).

Eq. (4) calls for a value of a_{v}. The catalytic surface area per unit suspension volume can be calculated from two well-known system parameters: the catalyst loading ($C_{\mathrm{m,cat}}$) and the catalyst specific surface area (S_{g}):

$$a_{\mathrm{v}} = C_{\mathrm{m,cat}} S_{\mathrm{g}} \tag{9}$$

The product $a_{\mathrm{v}} r_{i,\mathrm{het}}$ that is required for the mass balance (Eq. (4)) is obtained by multiplying Eq. (8) with Eq. (9). After rearranging

$$r_{i,\mathrm{het}}(\underline{x},t)a_{\mathrm{v}} = -S_{\mathrm{g}} C_{\mathrm{m,cat}} \alpha_1 \left(\frac{\alpha_3 C_i(\underline{x},t)}{1+\alpha_3 C_i(\underline{x},t)}\right)^2 \times \left[\sqrt{1+\frac{\alpha_2 \int_\lambda e^{\mathrm{a}}_\lambda(\underline{x},t,C_{\mathrm{m,cat}})\,\mathrm{d}\lambda}{C_{\mathrm{m,cat}}[\alpha_3 C_i(\underline{x},t)/(1+\alpha_3 C_i(\underline{x},t))]^2}} - 1\right] \tag{10}$$

Let us assume that in every point ($\underline{x}$) inside the reaction space and at any time during the process, the following relationship is satisfied:

$$\alpha_2 \int_\lambda e^{\mathrm{a}}_\lambda(\underline{x},t,C_{\mathrm{m,cat}})\,\mathrm{d}\lambda \gg C_{\mathrm{m,cat}} \left(\frac{\alpha_3 C_i(\underline{x},t)}{1+\alpha_3 C_i(\underline{x},t)}\right)^2 \tag{11}$$

Then, in Eq. (10) the following equation holds:

$$\sqrt{1+\frac{\alpha_2 \int_\lambda e^{\mathrm{a}}_\lambda(\underline{x},t,C_{\mathrm{m,cat}})\,\mathrm{d}\lambda}{C_{\mathrm{m,cat}}[\alpha_3 C_i(\underline{x},t)/(1+\alpha_3 C_i(\underline{x},t))]^2}} - 1 \cong \sqrt{\frac{\alpha_2 \int_\lambda e^{\mathrm{a}}_\lambda(\underline{x},t,C_{\mathrm{m,cat}})\,\mathrm{d}\lambda}{C_{\mathrm{m,cat}}[\alpha_3 C_i(\underline{x},t)/(1+\alpha_3 C_i(\underline{x},t))]^2}} \tag{12}$$

In Appendix A, it is shown that Eq. (12) is valid for all operating conditions of the system under consideration. Substituting Eq. (12) in Eq. (10) and defining

$$\alpha = \alpha_1 \sqrt{\alpha_2} \tag{13}$$

one gets

$$r_{i,\mathrm{het}}(\underline{x}, t)a_{\mathrm{v}} = -S_{\mathrm{g}}\sqrt{C_{\mathrm{m,cat}}}\alpha\left[\sqrt{\int_{\lambda} e^{\mathrm{a}}_{\lambda}(\underline{x}, t, C_{\mathrm{m,cat}})\,\mathrm{d}\lambda}\right] \times\left[\frac{\alpha_3 C_i(\underline{x}, t)}{1+\alpha_3 C_i(\underline{x}, t)}\right] \quad (14)$$

It should be noted that only under the conditions defined in Eq. (11) the photocatalytic reaction rate exhibits the following typical characteristics: (i) the rate is proportional to the square root of the LVRPA and (ii) a Langmuir–Hinshelwood type of expression is obtained for the substrate concentration dependence.

2.3. Local volumetric rate of photon absorption

To complete the information required by Eq. (14) we need the value of the LVRPA for the range of participating wavelengths. Monochromatic absorption rates are readily obtained if the field of monochromatic radiation intensities is known inside the reaction space. All what is needed is an integration over all the incoming directions according to

$$e^{\mathrm{a}}_{\lambda}(x, y, t) = \int_{\Omega=4\pi} I_{\lambda}(x, y, t, \Omega)\,\mathrm{d}\Omega \quad (15)$$

Monochromatic radiation intensities as a function of position, time and direction of propagation, $I_{\lambda}(x, y, t, \Omega)$, can be obtained from the solution of the radiative transfer equation (RTE) applied to this particular photoreactor. The flat plate configuration suggests the use of Cartesian geometry. As shown in Fig. 2(a), the lamp length is much larger than the reactor width (corresponding to the z coordinate). Consequently, since symmetry for the z-direction seems to be a plausible assumption, a two-dimensional model for spatial variations of the radiation field in the x- and y-directions is acceptable. Radiation propagation, as usual, is modeled with two spherical coordinates (θ, ϕ). With these considerations, the RTE for a 2D, rectangular space, including absorption and

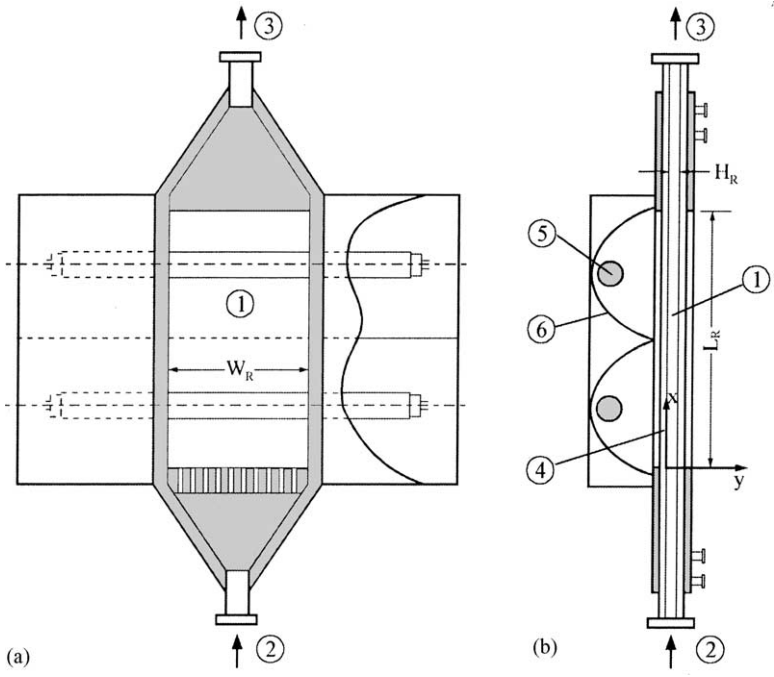

Fig. 2. Details of the experimental photoreactor: (a) front view; (b) side view. (1) Reaction space, (2) fluid in, (3) fluid out, (4) plate of radiation entrance, (5) UV lamp, and (6) parabolic reflector.

scattering is [6]

$$\mu\frac{\partial I_\lambda(x,y,\Omega)}{\partial x}+\eta\frac{\partial I_\lambda(x,y,\Omega)}{\partial y} = -(\kappa_\lambda+\sigma_\lambda)I_\lambda(x,y,\Omega) + \frac{\sigma_\lambda}{4\pi}\int_{4\pi} p(\Omega'\rightarrow\Omega)I_\lambda(x,y,\Omega')\,\mathrm{d}\Omega' \quad (16)$$

where μ and η are the direction cosines corresponding to the direction of propagation [$\Omega(\theta,\phi)$] with respect to the Cartesian axes x and y ($\mu = \cos\phi\sin\theta$, $\eta = \sin\phi\sin\theta$).

Eq. (16) must be solved with the appropriate boundary conditions in terms of radiation intensities as follows: (i) intensities at the irradiated reactor wall (x–z plane at $y = 0$); (ii) intensities at the opposite reactor wall (x–z plane at $y = H_R$), and (iii) intensities at the two lateral walls corresponding to x–y planes at $z = 0$ and $z = W_R$. Thus, we have the following:

1. Irradiated wall:

$$I_\lambda(x, y = 0, \Omega = \Omega_{in}) = \Im\ \text{(Properties of the emitting system and the reactor wall)} \quad (17)$$

2. Opposite reactor wall:

$$I_\lambda(x, y = H_R, \Omega = \Omega_{in}) = \Im\ \text{(Properties of the arriving radiation and the reactor wall)} \quad (18)$$

3. Lateral walls:

$$I_\lambda(x = 0, y, \Omega = \Omega_{in}) = 0 \quad (19)$$

$$I_\lambda(x = L_R, y, \Omega = \Omega_{in}) = 0 \quad (20)$$

Eqs. (19) and (20) indicate that no radiation is going inside the reactor from these walls. Ω_{in} represents all directions of radiation intensity entering the reactor.

Polychromatic operation may be easily modeled integrating monochromatic LVRPAs (Eq. (15)) over the employed wavelength interval.

As portrayed in Fig. 2, the reactor is irradiated with two tubular lamps placed at the focal axis of two cylindrical reflectors of parabolic cross-section. The employed lamps have superficial emission. The reactor receives direct radiation from two lamps and indirect radiation from two reflectors. This combined emission can be modeled. Hence, for radiation sources having superficial, diffuse emission and parabolic mirrors producing specular reflection the models has been described by Cassano et al. [9]. This mathematical representation provides values of radiation intensities resulting from the addition of the four contributions. This approach was used to optimize the geometrical arrangement (spatial organization of both emitting systems) in order to have an almost uniform radiation flux on the reactor surface [7]. The method provides values of radiation intensities on each point on the external side of the surface of radiation entrance. This information is not enough to calculate the first boundary condition. One must take into account that the reactor wall is a real surface that changes the amount of radiation arriving at the reactor volume. For either boundary condition (i) or (ii) reflection at all air–glass and glass–liquid interfaces, as well as absorption in the wall thickness must be computed. Additionally, it is well known that titanium dioxide tends to adhere to the glass wall, making necessary to account for the progressive fouling of the surface. These aspects of the modeling have been described in detail elsewhere [6].

2.4. Model parameters

Solution of the RTE requires information concerning several parameters of the model as follows: (1) dimensions and physical characteristics of the reactor, lamps and reflectors (they are provided in Table 1), (2) specific (per unit mass concentration) coefficients of absorption and extinction by the catalytic suspension as a function of wavelength (they are supplied in Table 2), (3) corrections of the values of these two properties as a function of time as it will be described in Section 4 of this paper, (4) the phase function for scattering that according to Brandi et al. [6] has been assumed isotropic ($p = 1$), and (5) intrinsic kinetic parameters corresponding to the kinetic model of the photocatalytic reaction (values of α and α_3). Values reported in Table 2 for Aldrich titanium dioxide were obtained according to the procedure described in [10]. The values of α and α_3 will be calculated from all the experimental information that has been obtained in this work.

Table 1
Reactor and emitting system characteristics

	Value	Units
Reactor		
Length	34.0	cm
Width	18.0	cm
Thickness	1.2	cm
Irradiated volume	734.4	cm^3
Wall thickness	0.38	cm
Batch recycling system		
Total suspension volume	10,000	cm^3
Recirculating flow rate	5,280	cm^3/min
Lamps (two UV Philips TLK40/09N)		
Nominal power (each)	40	W
Output power (310 nm$\leq \lambda \leq$ 410 nm)	6.5	W
Diameter	3.8	cm
Nominal arc length	60	cm
Reflector (parabolic cross-section)		
Parabola characteristic constant	2.4	cm
Height	9.6	cm
Length	54.0	cm
Opening	19.2	cm

2.5. Numerical solution

Eqs. (1)–(7) and (14) represent a system of coupled ordinary differential equations (ODEs) that must be solved together with the integro-differential equation that describes the radiation field (Eqs. (15)–(20)). The numerical solution has recurred to a marching method as follows:

Table 2
Specific absorption and extinction coefficients for Aldrich TiO_2[a]

Wavelength (nm)	κ^* ($cm^2\ g^{-1}$)	β^*_{η} ($cm^2\ g^{-1}$)
295	8,356	35,291
305	8,531	35,630
315	8,797	35,877
325	8,922	36,473
335	8,995	37,328
345	8,340	38,359
355	6,435	39,392
365	3,045	40,307
375	951	40,769
385	379	41,433
395	239	42,245
405	193	42,773

[a] Note that $\beta^*_{\eta} - \kappa^* = \sigma^*$ (the specific scattering coefficient).

1. The starting concentration of TCE is used as the initial condition: $C^{ou}_{i,Tk}(t_0 = 0) = C^0_i$.
2. For a given time $t = t_N$ the ODE represented by Eqs. (4)–(6) is solved employing a fourth-order Runge–Kutta method and the following additional information:
   2.1. For every reaction time, the outlet concentration from the tank at $t = t_N$ is the inlet concentration to the reactor.
   2.2. The heterogeneous degradation rate is calculated with Eq. (14).
   2.3. The values of the LVRPA are calculated with Eqs. (15)–(20). At this point it must be noted that the calculation must incorporate, *at each different time* the measured changes in the optical properties of the system as it is described in Section 4.
3. With the TCE concentration profile at the reactor outlet (for the time t_N) and Eq. (7), the mixed-cup average concentration is calculated (pseudo-steady state approximation).
4. With a second-order Runge–Kutta integration algorithm the ODE represented by Eqs. (1) and (2) is solved. In this way one can obtain the outlet concentration from the tank for the next incremental time $t = t_{N+1}$.
5. Steps 2–4 are repeated as many times as needed to reach the final reaction time.

Two additional aspects of the calculation procedure must be commented. Firstly, the way used to select the employed time interval for our calculations ($\Delta t = t_{N+1} - t_N$). Starting from an arbitrarily chosen time interval the value of Δt was gradually decreased to a value where the model response (TCE concentration at the end of an hypothetical run) did not show variations with further decrements. Secondly, the method employed to calculate step 2.3 in the marching procedure. For the two-dimensional (x, y)–two directional (μ, η) model the solution of the RTE was obtained resorting to the discrete ordinate method (DOM) as described by Duderstadt and Martin [11]. The integro-differential equation (Eq. (16)) is transformed into a set of algebraic equations. The DOM takes into account the special characteristics of the phenomenon of radiation propagation that depends not only on position but also on the direction of the radiation ray trajectory. For application of the DOM the system must be made

discrete in three different variables: (i) spatial discretization in the x, y variables, (ii) directional discretization in the spherical variables [$\Omega = \Omega(\theta, \phi) = \Omega(\mu, \eta)$], and (iii) spectral discretization in the useful employed wavelengths (λ). This last operation resulting from the type of light used in the experiments since the utilized actinic lamps are polychromatic. More details on the DOM to solve the RTE can be found in [6,7].

3. Experimental

3.1. Setup

Figs. 2 and 3 provide a schematic representation of the experimental setup. As shown in Fig. 3 there are four main parts: (1) the flat plate photoreactor, (2) the illuminating system, (3) the recycle, with a tank, a heat exchanger and a centrifugal pump, and (4) a detector system to measure the radiation that is coming out of the reactor from the surface opposite to the one employed for radiation entrance.

The photoreactor geometry is similar to the one adopted in the previous work [6,7]. The main differences are: (1) This reactor was made entirely with borosilicate glass; i.e., all the surfaces in contact with the reacting mixture were made of glass in order to avoid any possible adsorption of TCE by other materials. (2) The thin rectangular parallelepiped was constructed with a glass frame that has a decreasing cross-section in both the income and outgoing sections. (3) The bottom edge for entrance has a specially designed fluid distribution system to improve flow uniformity along the reactor cross-sectional area. (4) Sealing of the reactor flat surfaces (borosilicate glass; 3.8 mm) with the glass frame was achieved with a very thin silicone ring. Fig. 2 and Table 1 show the principal characteristics of this design.

Irradiation was produced by two emission modules. Each one of them is formed by one tubular, actinic lamp (UV Philips TLK40/09N) with superficial, diffuse emission that is placed at the focal axis of a cylindrical reflector of parabolic cross-section. Reflectors were custom made with mirror type, specularly finished aluminum sheet with Alzak® treatment provided by Alcoa. The whole illuminating system is placed inside a metallic box that permits the careful control of the position of the lamp and the reflector with respect to the reactor and ensures the reproducibility of the generated radiation field. The box is separated from the reactor by means of a shutter that can be removed to start the reaction once steady state operation of the whole system has been achieved (lamp operation, flow rates, temperatures, etc.).

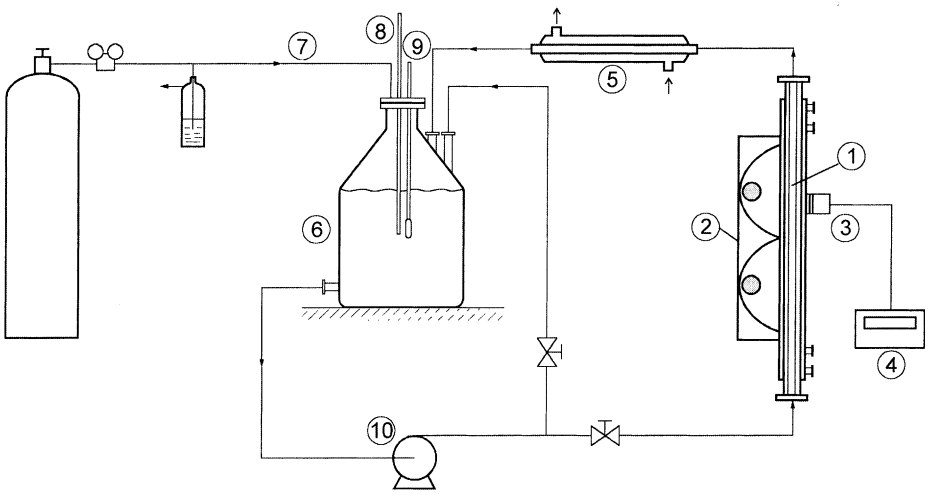

Fig. 3. Experimental device: (1) photoreactor, (2) emitting system, (3) UV sensor, (4) radiometer, (5) heat exchanger, (6) storage tank, (7) oxygen inlet, (8) liquid sampling, (9) thermometer, and (10) centrifugal pump.

As shown in Fig. 3, the reactor operated inside a recycle that has: (1) an all glass heat exchanger connected to a thermostatic bath (to control the operating temperature), (2) an all glass centrifugal pump (QVF) actuated by a variable speed motor, and (3) a 15 l storage tank also made of glass. The tank has provisions for: (i) temperature measurement, (ii) a constant pressure, continuous feed for oxygen intake, and (iii) a sampling port. The pump was used to recirculate the liquid to and from the reactor and to produce a secondary but important flow rate that leaves and goes back to the tank to improve mixing and facilitate the oxygen uptake. All connecting lines are made of glass. The tank and the connecting lines were masked with black tape to prevent the photoreaction to occur in a different place than the reactor.

To be able to quantify the change in the optical properties of both the reactor walls and the suspension, radiation fluxes were determined at the plate opposite to the surface of radiation entrance. Radiation fluxes coming out of the reactor flat surface were measured by means of an IL1745 UV Curing Radiometer (International Light) that can be used with different UV sensors. The detector has an automatic range along 10 decades with a ±0.1% linearity ($1–1 \times 10^{-9}$ W cm^{-2}). The sensor was a SED005/WBS320/W (International Light). It is made with a photodiode GaAsP type, having an active area of 5 mm^2 coupled with a bandpass filter (WBS320) and a wide eye diffuser (W) made of quartz. The sensor window is 42 mm in diameter and has a spectral range from 250 to 400 nm with a peak at 350 nm (PIR $= 9.3 \times 10^{-4}$ A W^{-1} cm^2). The directional response (using the diffuser) follows the “cosine law”. A mechanical device permitted the exact positioning of the detector on different selected points of the reactor surface. In this way, at different positions on the x–z plane radiation fluxes can be precisely measured. More details on these procedures can be found in [6,12].

3.2. Procedure

For each run a stock solution of TCE was prepared. The 500 ml of pure water (18 MΩ) were placed in a glass ampoule to which a small volume of TCE (99.9%, Carlo Erba, RSE) was added. After vigorous stirring the mixture was left for 12 h in a thermostatic bath at 20 °C. In this way a saturated solution of TCE in water was obtained that has 1076 ppm of TCE [13]. This value was verified with GC analysis employing a standard solution of TCE in carbon sulfide.

Each run begins by filling the reactor and the tank with a prescribed amount of water that is saturated with oxygen, recirculated in the system and stabilized at 20 °C. This operation takes about 30 min. The lamps are switched on and after about 30 min of operation and temperature stabilization, with the lamps shutter off, radiation transmitted by pure water is recorded with the UV detector. This corresponds to the conditions of “clean” reactor walls. Then, the lamp shutter is placed on and the desired amount of the stock solution of TCE is added to the reactor. Samples of the reacting mixture are taken after recirculation during several minutes (10 min time interval) to make sure that the TCE concentration in pure water has reached a stable value (this corresponds to the “feed concentration of TCE”). Then, the required amount of catalyst is incorporated to 500 ml of pure water, sonicated for 1 h and afterwards added to the system. At this time, the radiation transmitted by the suspension is measured again (transmission for the loading time $t = t_l$). The suspension is recirculated for about 1 h and left overnight to permit the system to reach the dark adsorption equilibrium (minimum of 12 h). The next day the oxygen feed is turned on, the lamps are turned on (lamp shutter on) and recirculation starts again until steady state conditions of flow rates and temperature are reached. The concentration of TCE is measured again at time intervals of 1 h. When a constant value is obtained (after complete adsorption) one can consider that this value corresponds to the “initial TCE concentration” in the liquid. At this moment the shutter is turned off and the observed transmission characteristics of the suspension are recorded as the initial optical conditions of the catalyst. This is also taken as the time $t = 0$ of the experimental run. Every 30 min concentration of TCE was measured with GC employing FI detectors and, at different time intervals, transmission characteristics of the suspension were recorded. During each experiment the temperature is kept at 20 °C and the lamp operation is monitored with a V-A-W meter.

At the end of each run the reactor is emptied from the reaction suspension and filled with pure water. The transmission characteristics of the used reactor walls (with titanium dioxide fouling) are recorded to compare this value with the conditions of clean wall.

4. Optical properties of the suspension

As mentioned before the transmission characteristics of the reactor volume has significant changes along the duration of a run (approximately 4 h). This change must surely affect the volumetric rate of photon absorption at different points inside the reactor; because of this, it translates into the reaction rate. Changes in the transmission properties of the reactor wall leads to a decrease in the transmitted radiation registered by the detector. Conversely, alteration in the suspension (agglomeration) produces the opposite effect. It was also observed that working with Aldrich titanium dioxide the consequence of the fouling of the reactor walls can be considered a perturbation of second order compared with the modification in the transmission of the reactor produced by alteration of the optical properties of the suspension (see also [6]). It was decided to concentrate the empirical corrections on this last effect.

The change in the optical characteristics of the suspension seems to be due to two principal causes [8]: (i) suspension pH and (ii) stirring and/or circulation through a pump. At pH's close to the isoelectric point (ca. 6.4) titanium dioxide particles show the maximum agglomeration, whereas working at higher or lower pH's the effect is reduced. During the reaction the pH goes from an initial value of 6 to a final value that depends on the conversion may be as low as 3. Stirring and/or recirculation always produce agglomeration that is less important away from the isoelectric point.

One can assume that a modification in the extinction coefficient ($\beta_\lambda = \kappa_\lambda + \sigma_\lambda$) produced in the reaction suspension is mainly due to changes in scattering centers size that will affect more severely the scattering characteristics of the slurry. One can further assume that on the contrary, working with specific coefficients (per unit solid mass concentration), the absorption characteristics should be less altered because absorption is directly related to the semiconductor band gap and much less influenced by the particle size. Then one can attribute all changes in extinction to modifications in the scattering properties.

In order to evaluate quantitatively these changes, extinction by the suspension was measured with the detector placed at the reactor wall that is opposite to the wall of radiation entrance. The detector described in Section 3.1 was located at seven different positions along the x coordinate (Fig. 3) and transmission was measured at different catalyst concentrations. In Fig. 4, "transmission by the reactor" for four different catalyst concentrations has been plotted as a function of the reaction time. Reactor transmission has been defined as

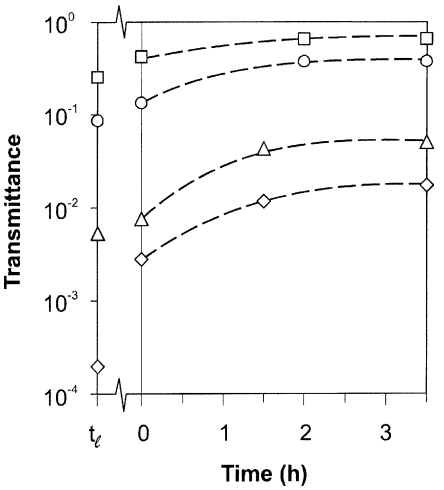

Fig. 4. Experimental transmittance of the flat plate reactor vs. time, for different catalyst loadings: (□) $C_{m,cat} = 0.05$ g/l, (○) $C_{m,cat} = 0.1$ g/l, (△) $C_{m,cat} = 0.05$ g/l, (◇) $C_{m,cat} = 0.1$ g/l.

$$T(t, C_{m,cat}) = \frac{\text{Transmitted radiation flux at time } t \text{ and loading } C_{m,cat}}{\text{Transmitted radiation flux at time } t \text{ and } C_{m,cat} = 0 \text{ (pure water)}} \quad (21)$$

A semi-logarithmic plot has been used in Fig. 4 in order to show with a better representation the important changes that have been observed. Note that the moment in which the suspension has been loaded to the reactor has been indicated as $t = t_l$, whereas the time $t = 0$ has been used to indicate the moment in which the photocatalytic reaction itself commences. Properties of the catalytic suspension for the time $t = t_l$ are the ones listed in Table 2; i.e. unmodified optical properties (after sonication). Note also that between $t = t_l$ and $t = 0$ there is a minimum of 12 h (overnight elapsed time for adsorption equilibrium).

It can be seen that during the first 2 h there is a significant increment in transmission. This increment is larger when the catalyst concentration is higher: from

1.5 times at $C_{m,cat} = 0.05$ g/l to 60 times when the catalyst loading is 1 g/l. After the first 2 h changes tend to become negligible and one can safely consider that the optical properties are almost constant. But these results show that it is very important to incorporate these modifications during the initial steps of the reaction.

Changes in the specific extinction coefficient are calculated according to

$$\beta^*(t, C_{m,cat}) = \beta^*(t_l, C_{m,cat})\Im_{corr}(t, C_{m,cat}) = \beta^*_{t_l}\frac{\ln T(t, C_{m,cat})}{\ln T(t_l, C_{m,cat})} \quad (22)$$

The value of $\beta^*_{t_l}$ is obtained from Table 2 and the transient correction is obtained from Fig. 4. In the model, these changes are attributed exclusively to the specific scattering coefficient.

5. Results and discussion

Several experimental runs were made with the following range of values for the investigated variables: (i) three levels in the TCE initial concentration (25, 50 and 100 ppm) and (ii) four levels of catalyst concentration (0.05, 0.10, 0.50 and 1 g/l).

The kinetic parameters of Eq. (14) (α and α_3) were estimated from all the TCE concentration vs. time experimental data applying a non-linear regression procedure. The numerical method makes use of the following information: (i) theoretical predictions of TCE concentration vs. time obtained from the integration of the mass balances described in Section 2.1, (ii) the kinetic model represented by Eq. (14) in Section 2.2, (iii) the LVRPA obtained from the solution of the RTE in the rectangular reaction space, employing the DOM, (iv) the optical parameters of the system (for solving the RTE) that are known as a function of wavelength and time (Eq. (22) and Table 2), and (v) the measured values of TCE concentration vs. time for the complete set of experimental runs. Table 3 gives the values of the two kinetic parameters.

Figs. 5 and 6 show the results derived from inserting the estimated parameters in the model and a comparison with the experimental data. Fig. 5 shows the temporal evolution of the TCE concentration for the lowest catalyst concentration (0.05 and 0.1 g/l) and Fig. 6 for the highest (0.50 and 1.0 g/l). In these figures, the solid circles, triangles and squares represent the "feed" TCE concentrations that are different from the "initial" TCE concentrations because in the former adsorption has not taken place yet.

Table 3
Values of the kinetic parameters

Kinetic parameter	α (mol g$^{1/2}$ cm^{-2} s$^{-1/2}$ einstein$^{-1/2}$)	α_3 (cm^3 mol^{-1})
Value	1.94×10^{-9}	5.52×10^6
95% confidence interval	$\pm 0.10 \times 10^{-9}$	$\pm 0.67 \times 10^6$

It is seen that increasing the initial concentration of TCE leads to a slight decrease in the final conversion. For example, for a run that lasted 3.5 h and a catalyst loading of 0.5 g/l, employing initial concentrations equal to 23.0, 40.7 and 80.3 ppm, the measured final conversions were 0.42, 0.40 and 0.37, respectively. Also, it is observed that increasing the catalyst concentration the substrate conversion increases significantly. For example, for an initial TCE concentration of 40 ppm and the following catalyst loadings: 0.05, 0.10, 0.50 and 1.0 g/l, the final TCE conversions after 3.5 h are 0.13, 0.21, 0.40, and 0.56, respectively.

Looking at all the plots it can be deduced that the kinetic model represents in a fairly good manner the observed experimental data. It can be seen that, except for the case of a catalyst loading of 1.0 g/l and very low TCE concentrations, the percentage error is never larger than 18.2%.

For the same reaction but employing: (i) a quite different reactor, (ii) a different radiation source, (iii) a different phase function for scattering, (iv) different optical parameters for the catalytic suspension, and (v) a different batch of the Aldrich titanium dioxide, the following kinetic constants for Eq. (8) have been reported [3]:

$$\alpha_1 = 2.46 \times 10^{-14}\ (\text{mol cm}^{-2}\,\text{s}^{-1}),$$
$$\alpha_2 = 1.57 \times 10^{11}\ (\text{g s einstein}^{-1}),$$
$$\alpha_3 = 6.42 \times 10^{6}\ (\text{cm}^3\,\text{mol}^{-1})$$

From Eqs. (13) and (14) it can be deduced that for comparing these values of the kinetic parameters with the ones extracted from this work one must note that constants α_1 and α_2 corresponding to Cabrera et al.'s work [3] have collapsed to a single constant α in this

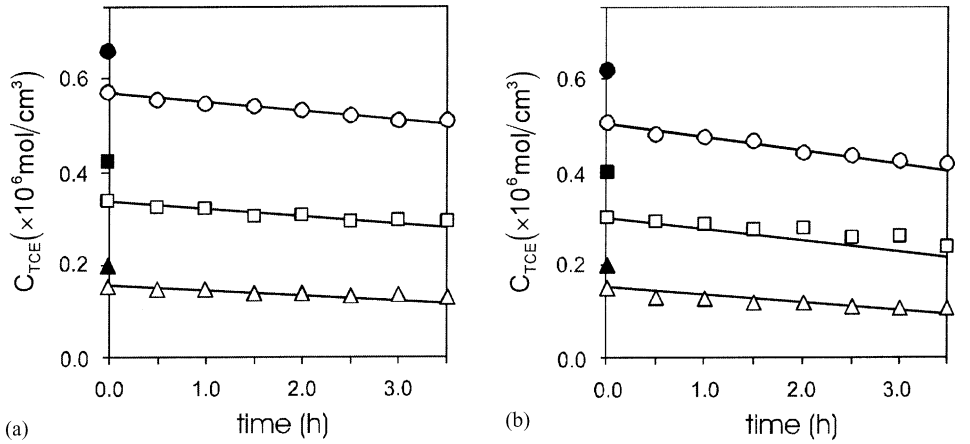

Fig. 5. TCE concentration vs. time for different catalyst concentrations: (a) $C_{m,cat} = 0.05$ g/l, (b) $C_{m,cat} = 0.10$ g/l. (—) Theoretical model; (△), (▲), (□), (■), (○) and (●) experimental points.

work. Then,

$$\alpha_1\sqrt{\alpha_2} = 9.75 \times 10^{-9} \times (\text{mol g}^{1/2}\,\text{cm}^{-2}\,\text{s}^{-1/2}\,\text{einstein}^{-1/2})$$

We can now compare: (i) the value of α (this work) with the product of $\alpha_1\sqrt{\alpha_2}$ from Cabrera et al. [3] and (ii) the value of α_3 in both reports. It can be seen that they are not equal but in both cases the order of magnitude is preserved.

Among the different causes for these differences one can list:

1. The wavelength distribution of the lamp: the wavelength distribution of the employed lamp is different than that corresponding to the ones employed here. Within the range of absorption by titanium dioxide (and transmission by the reactor glass walls) the lamp employed in [3] is richer in shorter wavelengths, a fact that should result in higher reaction rates [14].

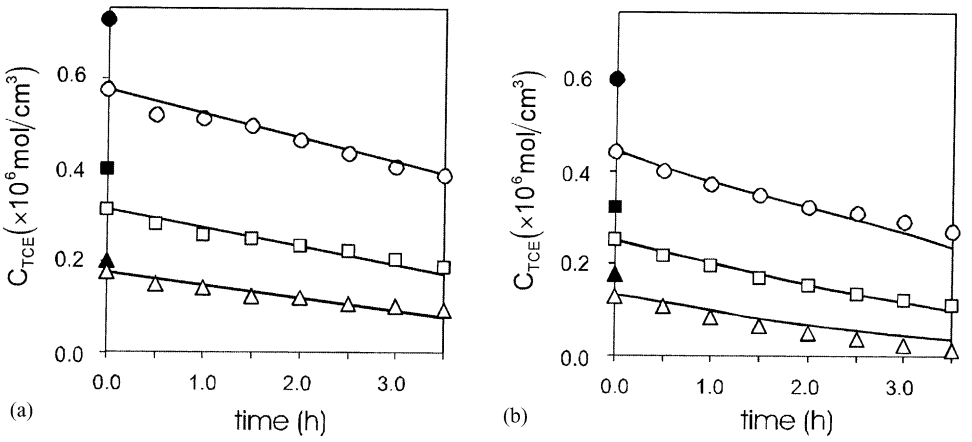

Fig. 6. TCE concentration vs. time for different catalyst concentrations: (a) $C_{m,cat} = 0.50$ g/l, (b) $C_{m,cat} = 1.0$ g/l. (—) Theoretical model; (△), (▲), (□), (■), (○) and (●) experimental points.

2. The batch of Aldrich titanium dioxide: the results obtained in [3] are restricted to the batch of Aldrich TiO_2 employed in that work (which is not necessarily exactly equal to the one employed here) and certainly cannot be extended to other varieties of the catalyst. Differences produced by different batches of titanium dioxide are difficult to foresee.
3. The optical parameters: the optical parameters employed in both studies are different. These differences are translated to the values of the estimated kinetic parameters. Three aspects must be considered:
   3.1. This work used the isotropic phase function for scattering ($p = 1$), while Cabrera et al. [3] had used the diffuse function [$p = (8/3)(\sqrt{1-\vartheta^2} - \vartheta \cos^{-1}\vartheta)$ and $\vartheta = \vartheta(\mu, \eta)$]. As indicated before, Brandi et al. [6] have shown that the isotropic scattering represents better the scattering produced by titanium dioxide.
   3.2. For the initial conditions with "fresh" suspension of titanium dioxide ($t = t_1$) we have used here the absorption and scattering coefficients reported in [6]. These coefficients were obtained employing the same method and experimental setup reported in [10] but using the isotropic phase function in their estimation. Cabrera et al.'s work [3] used coefficients that were estimated employing the diffuse phase function for scattering.
   3.3. During the reaction, i.e., for times $t > t_1$, the present radiation model takes into account the variations in the optical properties of the suspension with time, resulting from the unavoidable agglomeration produced by recirculating the catalyst, particularly during the first 2 h of operation. This correction, that is significant, was not considered in previous work.

One can conclude that the kinetic parameters reported in this work are acceptable and perhaps even more accurate than the ones previously reported and that the problem derived from using a different batch of titanium dioxide cannot be accounted for by the present state of our knowledge on photocatalytic reactions.

6. Conclusions

The results from this work can be summarized in the following statements:

1. A kinetic model for TCE photo-oxidation that includes explicit functional dependencies for the LVRPA and the catalyst concentration effects was satisfactorily validated with experiments.
2. The kinetics of the TCE photocatalytic degradation under usual operating conditions (low substrate concentration, typical catalyst loadings, aerated water, intermediate to high irradiation rates, no mass transport limitations, etc.) can be well represented by two lumped kinetic constants.
3. These results are valid for operating conditions where the oxygen concentration is always in excess at all points inside the reactor, i.e., this model does not account for the effect of oxygen on the kinetics.
4. The derived kinetic constants are valid for scaling-up if the spectral distribution of the laboratory and industrial lamp are similar; for precise calculations the effects of the wavelength distribution of different radiation sources cannot be neglected. This limitation results from the lack of information concerning the values of the primary quantum yield for electron–hole generation as a function of wavelength. In this work (see [2]) an average value over wavelengths has been assumed.
5. The same statement applies to the optical properties employed in the modeling; i.e., absorption and scattering coefficients may show changes if different methods of interpreting the experimental results are employed; i.e., a different adopted phase functions for scattering will render different coefficients.
6. The optical properties of the reaction space change during the process. They are important during the first 2 h and cannot be neglected.
7. Reactor wall fouling by Aldrich titanium dioxide, under our operating conditions, is not very important. This statement cannot be generalized to other varieties of titanium dioxide and perhaps to other concentrations.
8. It is also clear that reproducible results beyond an order of magnitude approximation are very hard to reach if different batches of the catalyst are used in different experiments; a universal problem for almost any catalytic system.

9. With the above mentioned limitations, these results are extrapolative to any other reactor geometry and/or configuration.

Acknowledgements

The authors are grateful to Universidad Nacional del Litoral, Consejo Nacional de Investigaciones Científicas y Técnicas, Agencia Nacional de Promoción Científica y Tecnológica and the CYTED program for their support to produce this work. Thanks are also given to Eng. Claudia M. Romani for technical assistance and to Lic. Diana E. Pedulli for her valuable help in part of the experimental work.

Appendix A

Eq. (11) in the main body of this paper can be written in a different form

$$\frac{\alpha_2 \int_\lambda e^{a}_\lambda(x,t,C_{m,cat})\,d\lambda}{C_{m,cat}[\alpha_3 C_i(x,t)/(1+\alpha_3 C_i(x,t))]^2} \gg 1 \qquad (A.1)$$

One way of verifying this assumption is to calculate the minimum possible value of the left-hand side (LHS) of Eq. (A.1) for our experimental operating conditions and see if it is much greater than 1. If the above condition is satisfied, the simplification thereby derived will hold for any other investigated variables and parameters. The minimum of the function in the LHS will be obtained for: (i) the maximum value of $C_{m,cat}$, (ii) the LVRPA in the internal side of the wall opposite to the one for radiation entrance, i.e., $e^{a}_\lambda(L_R,t)$, and (iii) for $C_{TCE} = C^0_{TCE}$ and choosing the maximum employed initial concentration in the experimental program.

Considering previously published values of the kinetic constants for α_2 and α_3 [3] and calculating all other variables and parameters as indicated below

$C_{m,cat} = 1.0\,g/l = 1.0 \times 10^{-3}\,g\,cm^{-3}$,

$e^{a}_\lambda(L_R,t) = 2.9 \times 10^{-13}\,einstein\,cm^{-3}\,s^{-1}$ (calculated at $x = L_R$),

$C^0_{TCE} = 80.3\,ppm = 0.61 \times 10^{-6}\,mol\,cm^{-3}$

and substituting into Eq. (A.1) it is obtained that

$$\left[\frac{\alpha_2 \int_\lambda e^{a}_\lambda(x,t,C_{m,cat})\,d\lambda}{C_{m,cat}[\alpha_3 C_i(x,t)/(1+\alpha_3 C_i(x,t))]^2}\right]_{min} \cong 72 \qquad (A.2)$$

This value corresponds to the most critical condition. As a way of an example, if one repeats the calculation for a catalyst loading of $C_{m,cat} = 0.1\,g/l$ the value of the function on the LHS of Eq. (A.1) is 7.8×10^6.

References

[1] R.J. Brandi, O.M. Alfano, A.E. Cassano, J. Adv. Oxid. Technol. 4 (1999) 76.
[2] O.M. Alfano, M.I. Cabrera, A.E. Cassano, J. Catal. 172 (1997) 370.
[3] M.I. Cabrera, A.C. Negro, O.M. Alfano, A.E. Cassano, J. Catal. 172 (1997) 380.
[4] C.S. Turchi, D.F. Ollis, J. Catal. 122 (1990) 178.
[5] A.E. Cassano, O.M. Alfano, Catal. Today 58 (2000) 167.
[6] R.J. Brandi, O.M. Alfano, A.E. Cassano, Chem. Eng. Sci. 54 (1999) 2817.
[7] R.J. Brandi, O.M. Alfano, A.E. Cassano, Chem. Eng. Sci. 51 (1996) 3169.
[8] C.A. Martín, M.A. Baltanás, A.E. Cassano, J. Photochem. Photobiol. A 76 (1993) 199.
[9] A.E. Cassano, C.A. Martín, R.J. Brandi, O.M. Alfano, Ind. Eng. Chem. Res. 34 (1995) 2155.
[10] M.I. Cabrera, O.M. Alfano, A.E. Cassano, J. Phys. Chem. 100 (1996) 20043.
[11] J. Duderstadt, W. Martin, Transport Theory, Wiley, New York, 1979.
[12] R.J. Brandi, O.M. Alfano, A.E. Cassano, Environ. Sci. Technol. 34 (2000) 2631.
[13] A.L. Pruden, D.F. Ollis, J. Catal. 82 (1983) 404.
[14] M.A. Grela, M.A. Brusa, J.A. Colussi, J. Phys. Chem. B 101 (1997) 10986.